



Electrokinetic ion transport at micro–nanochannel interfaces: applications for desalination and micromixing

Wei Liu¹ · Yueting Zhou¹ · Pengpeng Shi^{2,3}

Received: 8 July 2019 / Accepted: 24 October 2019 / Published online: 8 November 2019
© King Abdulaziz City for Science and Technology 2019

Abstract

The ion concentration polarization (ICP) phenomenon occurs widely near nano-channel/membrane interfaces. Due to its extraordinary selective ion transport ability, ICP has been applied in many fields, such as desalination, molecular pre-concentration and biomolecular separation. This paper is devoted to describing the transport mechanism of buffer ions at micro–nanochannel interfaces. Here, a multiphysics coupling model is proposed, where the boundary condition for the fixed surface voltage is introduced to describe the effect of nanochannel networks. The effectiveness of the proposed model and the calculation process is confirmed through comparative simulations. Comparing the simulations with experimental ICP results shows that the proposed model can effectively describe the nonlinear distribution of electric fields and a typical vortex pair from flow phenomena. An analytic scaling law for the propagating ion depletion zone (IDZ) is proposed, and a theoretical analysis and numerical results confirm its existence. For transient evolution, the IDZ spreads as \sqrt{t} due to diffusion for $t < 0.01$ s and as t due to convection from 0.01 s $< t < 0.1$ s. Furthermore, detailed studies are performed to elucidate the ICP mechanism for desalination. The factors affecting desalination are investigated, including the buffer concentration, length and performance of the nanochannel network, height of the microchannel and the tangential electric field. Finally, the proposed research confirms that this device also has excellent potential as a micromixer pump. The rapid mixing of neutral particles can be realized using nonlinear electrokinetic flows with a mixing efficiency reaching 91%. The presented results provide some important guidance and physical insights into the design and optimization for this kind of chip and other related applications.

Keywords Ion concentration polarization · Micro–nanochannel · Propagating ICP · Electroosmotic flow · Concentration microchip

✉ Yueting Zhou
zhouyt@tongji.edu.cn

✉ Pengpeng Shi
shipengpeng@xjtu.edu.cn

¹ School of Aerospace Engineering and Applied Mechanics, Tongji University, Shanghai 200092, People's Republic of China

² School of Civil Engineering and Institute of Mechanics and Technology, Xi'an University of Architecture and Technology, Xi'an 710055, Shaanxi, People's Republic of China

³ State Key Laboratory for Strength and Vibration of Mechanical Structures, Shaanxi Engineering Research Center of NDT and Structural Integrity Evaluation, School of Aerospace, Xi'an Jiaotong University, Xi'an 710049, Shaanxi, People's Republic of China

List of symbols

C_0	Buffer concentration (M)
C_i	Ion concentrations (M)
C_m	Nanochannel surface concentration (M)
C_{\max}	Maximum in concentration mixture (M)
D	Diffusion coefficient (m^2/s)
E	Electric field (V/m)
e	Elementary charge (C)
F	Faraday's number (C/mol)
g	Gravitational acceleration (m/s^2)
H	Characteristic length (m)
J_i	Ion flux ($\text{mol}/\text{m}^2 \text{ s}$)
L	Microchannel length (m)
L_m	Nanochannel network length (m)
P	Pressure (Pa)
R	Gas constant ($\text{J}/(\text{mol K})$)
r	Index of mixing
T	Absolute temperature (K)
U	Fluid velocity (m/s)

V_L	Voltage at the left end of the channel (V)
V_{sur}	Surface voltage (V)
V_R	Voltage at the right end of the channel (V)
V_T	Thermal voltage (V)
Z_i	Ion valence
σ_-	Negatively charged density (mC/m^2)

Greek symbols

β	Coefficient of expansion (kg/mol)
ϵ_0	Vacuum permittivity (F/m)
$\epsilon_r(c)$	Solvent permittivity (F/m)
ϵ_w	Relative dielectric constant (1)
$\zeta(c)$	Zeta potential (V)
$\eta(c)$	Dynamic viscosity (Pa s)
$\rho(c)$	Concentration-dependent density (kg/m^3)
ρ_0	Initial fluid density (kg/m^3)
ρ_e	Space charged density (C/m^3)
Φ	Electric potential (V)

Subscripts

1	Cations
2	Anions
3	Particles

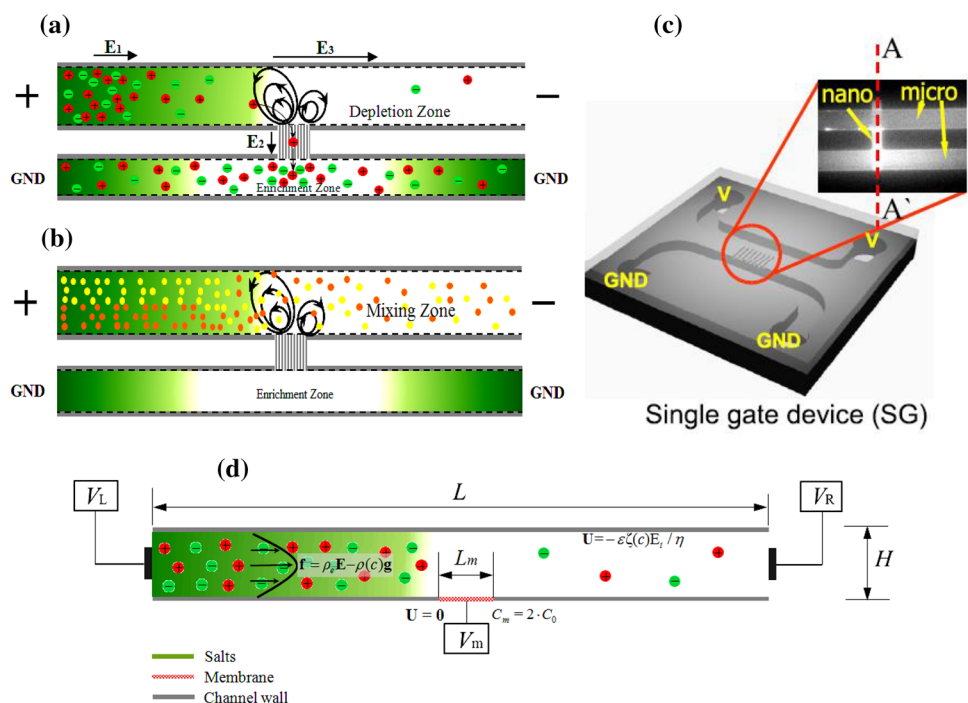
Introduction

When a series of nanofluidic channels are used to connect two microscopic channels, the electrolyte solution is forced to pass through the nanochannels when subjected to a tangential electric field (E_1). Overlapping electric double layers

(EDLs) cause nanofluidic channels to have an ion-selective functionality, which can cause the accumulation/enrichment of charged species on one side and a depletion on the other side of the micro–nanochannel in a process known as ion concentration polarization (ICP). As shown in Fig. 1a, b, the ICP induces a normal electric field (E_2), which in turn triggers vortices in the micro–nanochannel interfaces. Based on its ion depletion and vortex characteristics, the micro–nanochannel has been widely used as a seawater desalination chip (Nikonenko et al. 2014; Kim et al. 2010; Deng et al. 2015), concentration micromixer pump and other applications, attracting widespread attention from researchers.

Desalination has the greatest potential application for concentration microchips. For example, the process of converting salt to fresh water via ICP has been previously reported (Kim et al. 2010). During operation, both salt solutions and larger contaminant particles are pushed away from the ion selective nanochannels. A promising desalination technology is proposed by combining capacitive deionization with a battery system, which has a rapid ion removal rate and an excellent stability in an aqueous sodium chloride solution (Lee et al. 2014). In addition, the electrochemically mediated desalination of seawater was presented numerically by Hlushkou et al. (2016), but its desalination efficiency was far lower than that of the ICP (Kim et al. 2010). To improve the desalination efficiency, it is necessary to further analyze the mechanism and influencing factors of ICP desalination through both experimental and theoretical studies. The first direct measurements for the detailed flow and electric potential profiles within and near the ion depletion zone (IDZ)

Fig. 1 Schematic diagram for concentration micro–nanofluidic systems. **a** A desalination microchip consisting of two microchannels connected via a nanochannel network. **b** A micro-mixer chip based on nonlinear electroosmotic flow in the same micro–nano channels. **c** Concentration chip designed by Kim et al. (2007). **d** Physical model for the concentration chip. The microchannel contains a nanochannel network centered at its bottom, and the nanochannel surfaces with a fixed cation concentration and an applied voltage describe the effects of the nanochannel network



were reported by Kim et al. (2009). The measurements confirmed that the electric field inside the IDZ is amplified more than 30 times compared with the field outside the IDZ. However, there are many difficulties when measuring the full set of data (ion concentration and ion flux) in micro–nanochannels. Theoretical and numerical simulations are needed to further understand ICP phenomena.

For the ICP, a one-dimensional numerical analysis was performed by Dukhin (1991). The results showed that the tangential electric field exerts a force on the local space charge layer, leading to liquid movement along the interface analogous to an electroosmotic slip. Rubinstein and Zaltzman (2000) developed a theoretical model to analyze the electroconvective instabilities near a horizontal permselective surface. Based on a similar mathematical framework, a number of computational works using direct numerical simulation (DNS) have been performed using the Poisson–Nernst–Planck and Navier–Stokes equations. Their results indicated that the perturbed ion concentration layer induces a non-uniform electric field, which then triggers a stable vortex (Dydek et al. 2011; Pham et al. 2012) or even chaotic vortices (Shi and Liu 2018; Demekhin et al. 2013; Luo et al. 2016). Theoretically, Rubinstein and Zaltzman indicated that relaxing the assumption of perfect ion selectivity allows for equilibrium electroconvective instabilities (Rubinstein and Zaltzman 2015). A comprehensive numerical analysis of the transport processes associated with electrohydrodynamic chaos was presented by Druzgalski et al. (2013), which demonstrated that these instabilities have significant impacts as the flow behavior transitions from coherent vortex pairs to fully chaotic multi-layer vortex structures.

Experimentally, the nonlinear electrokinetic flow across a nanoporous membrane was studied by Yossifon and Chang (2008), who revealed that the thickness of the ion depletion zone (IDZ) obeys a self-similar scaling law of \sqrt{Dt} . Here, D is the diffusion coefficient and t is the time. Mani et al. (2009) and Zangle et al. (2009) developed a one-dimensional concentration shockwave equation to describe the depletion propagation. For a constant current model, they found that the enrichment and depletion zone propagation spread as t . However, for a constant voltage model, Zangle et al. (2010) found that the IDZ propagation spread as \sqrt{t} . In addition, Zangle et al. (2010) reviewed the current state of theory and experimental methods of CP propagation.

Based on the characteristics of an amplified electric field and nonlinear flow, micro–nano channels can be widely used to manipulate electrokinetic molecular concentrations. Duan and Majumdar (2010) estimated that the electrophoretic mobility (EPM) of monovalent ions in 2 nm hydrophilic nanochannels is four times larger than that for bulk solutions. In addition to the concentration boundary conditions of the membrane surface, the boundary condition of a fixed charge density was proposed by

Yeh et al. (2012). Based on a verified continuum-based model, the electric field-induced ion transport and the resulting conductance in a PE-modified nano-pore were investigated for the first time. Jia and Kim (2014) further used a similar model and boundary conditions to analyze the preconcentration of particles in micro–nanochannels. Their results indicated that the tangential electric field strength has an important effect on the enrichment of the particle concentrations. Shen et al. (2010) simulated the protein preconcentration process in a microchannel embedded with Nafion membranes. They used a constant zeta potential (Jia and Kim 2014; Shen et al. 2010) to describe the wall charge effect, but ignored the effects of the amplified zeta potential (Kim et al. 2009) on the particle preconcentration.

Recently, our group (Li et al. 2017) reported a multi-physics model that is distinct from the previous assumptions (using the surface charge density to describe charged sidewalls). Based on the multi-physics model, some new physical insights regarding the particle preconcentration phenomenon were obtained, such as the mechanism of particle enrichment and replacement of particles for buffer co-ions. More recently, Ouyang et al. (2018) performed a detailed experimental and theoretical analysis of the electrokinetic molecular concentration based on the previous multi-physics model. Using the flux equation for one-dimensional ion transport, they derived the scaling laws for the particle concentration. Their analyses also confirmed that the previous multi-physics model is reasonable under some certain assumptions. Unfortunately, a definition of the cross-nanochannel voltage V_{cm} was introduced in the previous model; however, it is difficult to define this in real experimental systems (Kim et al. 2009). Besides, the concentration chip can also be used for the design of a micromixer based on nonlinear electrokinetic flow (Mishchuk et al. 2009; Chiu et al. 2013; Choi et al. 2015); it is necessary to perform related research on transport mechanisms.

Numerical simulations for the full 3D analyses of the electrokinetic phenomena were performed by Adler's and Yi's group in Marino et al. (2001), Coelho et al. (1996) and Luo et al. (2018). Although researchers have carried out many numerical studies for the ICP, there is a large gap between the theoretical predictions and the experimental data. For example, Jia and Kim (2014) found a vortex on the nanochannel surface at a length of 100 μm . However, the length of the membrane or nanochannel network is only 4 μm in the majority of ICP experiments (Kim et al. 2009). For this common membrane at only around 4 μm in length, vortices cannot be obtained based on this previous theoretical model (Jia and Kim 2014). In addition, a linear variation of the voltage drop was discovered along the microchannel based on their model, which is different from the existing experimental results.

Here, we further investigate the numerical research on ICPs to explain the vortex generation and ICP desalination mechanism in channels with a feature length of 10 μm . In this paper, we employ the concentration-dependent zeta potential to describe the amplified zeta potential near the micro–nanochannel interfaces, in which a fixed surface voltage and a certain cation concentration are proposed to describe the nanochannel network. Then, a multi-physics coupling model for the concentration chip is established. Firstly, a reasonable theoretical model is developed to explain the mechanism of ion transport, where a fixed surface voltage is introduced to describe the effect of the nanochannel network. By neglecting the surface voltage boundary, an excellent agreement is obtained between the prediction from the proposed model and a previous model (Jia and Kim 2014). In particular, by comparing the results here with experimental results for the voltage distribution (Kim et al. 2009) and the vortex streamlines (Kim et al. 2008), it is confirmed that the surface voltage boundary condition is necessary to describe the effect of nanochannel networks.

Therefore, based on our proposed theoretical model, numerical simulations are systematically performed to discuss the effects of the buffer concentration, length and performance of the nanochannel network, height of the microchannel and tangential electric field on the desalination efficiency. We also identify mechanisms that propagate ICP under tangential electric fields. It is seen that the IDZ initially spreads as \sqrt{t} for $t < 0.01$ s and as t for 0.01 s $< t < 0.1$ s. Finally, the possibility of this concentration chip as a micromixer pump is evaluated. The proposed simulation may be helpful to understand the mechanism of ion transport near the micro–nanochannel interfaces and to advance the development of ICP applications.

Physical models

Figure 1b shows a schematic illustration of a micro–nanochannel ICP device in which the nanochannel network is integrated between two microchannels. In fact, the porous structure containing nanoscale pores with charged surfaces has the same ion-exclusion effects and ICP functionalities as a permselective membrane. In view of these facts, the hybrid micro–nanochannel model can be simplified as a model of two microchannels integrated with a membrane, where the membrane surface uses a fixed cation concentration and applied voltage to describe the effect of the nanochannel network. Based on the coupled governing equations with appropriate boundary conditions, one can investigate the non-equilibrium electrokinetic instability flow and IDZ near the nanochannel network.

The parameters for a concentration chip include a microchannel of length L and height H and a nanochannel network with length L_m centered at the bottom of the microchannel, as shown in Fig. 1d. The channel is filled with an electrolyte and, for simplicity, the system is assumed to be symmetric and binary (such as for NaCl). To achieve electroosmotic flow (EOF), an external electric field is often required for the system, which means that there is an electric potential difference at both ends of the microchannel. If the wall of the microchannel is negatively charged with a density σ_- , the number of cations in the microchannel is greater than that of the anions. The electric forces acting on the net charges in the solution induce an EOF from the left to the right; thus, the left end of the microchannel is referred to as the inlet and the right end as the outlet. The inlet of the microchannel is connected to a bulk solution, in which the concentrations of both cations and anions are equal at bulk concentration c_0 . Only the electrokinetic phenomena are studied here, so, for convenience, it is assumed that the pressures at both ends of the microchannels are zero and that only cations can pass through the surface of the nanochannel network under the applied voltage V_m . This assumption is consistent with a strong ion depletion effect, which means that a stronger vortex causes the cations to pass into the nanochannel network.

Theoretical modeling

Equations are provided in this section to establish the theoretical model for the electrokinetic transport simulation in two microchannels linked with a nanochannel network.

Concentration field

According to the theory of ionic transport, $c_1 = c_1(x, y, t)$, $c_2 = c_2(x, y, t)$ and $c_3 = c_3(x, y, t)$ denote the concentrations of the cations, anions and particles, respectively. The conservation laws for these species are

$$\frac{\partial c_i}{\partial t} = -\nabla \cdot \mathbf{J}_i, \quad (1)$$

where $\mathbf{J}_1 = \mathbf{J}_1(x, y, t)$, $\mathbf{J}_2 = \mathbf{J}_2(x, y, t)$ and $\mathbf{J}_3 = \mathbf{J}_3(x, y, t)$ are the associated fluxes; and $\nabla = (\partial/\partial x, \partial/\partial y)$ is the spatial gradient operator. Under the assumption of a dilute solution, the flux densities are expressed by the Nernst–Planck equations as

$$\mathbf{J}_i = -\left(D_i \nabla c_i + Z_i \frac{D_i F}{RT} c_i \nabla \Phi\right) + \mathbf{U} c_i, \quad (2)$$

where F is the Faraday's number, R is the ideal gas constant, T is the absolute temperature, $\Phi = \Phi(x, y, t)$ is the electric potential, $\mathbf{U} = \mathbf{U}(x, y, t)$ is the fluid velocity, Z_1 , Z_2 and Z_3 are the valences for the cations, anions and particles,

respectively, and D_1 , D_2 and D_3 are the diffusion coefficients of the cations, anions and particles, respectively.

Electric field

The electric potential can be determined from Poisson’s equation:

$$\nabla \cdot (\epsilon_r(c)\epsilon_0 \nabla \Phi) = -\rho_e, \tag{3}$$

where $\epsilon_r(c)$ is the permittivity of the solvent as a function of the ionic concentration and ϵ_0 is the vacuum permittivity. Here, the dielectric constant as related to concentration satisfies the following relationship: (Peng and Li 2015)

$$\epsilon_r(c) = \epsilon_w(1 - 3.742 \times 10^{-4}Tc + 0.034c^2 - 0.178c + 1.515 \times 10^{-4} - 4.029 \times 10^{-6}T^2),$$

where T is the temperature of the liquid ($^{\circ}\text{C}$), c is the ionic concentration (mM) of the solution, and ϵ_w is the relative dielectric constant of water at a reference temperature of $27\text{ }^{\circ}\text{C}$. So, the regular range of the relative dielectric constant for the NaCl solution is from 0.001 to 5 mol/L at the reference temperature of $27\text{ }^{\circ}\text{C}$.

As there are two kinds of charged ions, cations and anions, the charge density $\rho_e = \rho_e(x, y, t)$ can be expressed as

$$\rho_e = e(Z_1c_1 + Z_2c_2), \tag{4}$$

where e is the elementary charge, Z_1 is the cation valence, and Z_2 is the anion valence.

Duan and Majumdar estimated that the EPM of monovalent ions in 2 nm hydrophilic nanochannels is 4 times larger than that for bulk solutions (Duan and Majumdar 2010). Based on these experimental results, the EPM effects can be considered as similar to the previous model. For the membrane, a fixed volumetric charge on the surface of the nanochannel network is added to the right-hand side of the Poisson equation as $\nabla \cdot (\epsilon_r(c)\epsilon_0 \nabla \Phi) = -\rho_e - \rho_{\text{fix}}$ for the micro–nanochannel zone. Here, a ρ_{fix} of 0.001 mC/m^3 is used.

Flow field

The fluid in a microchannel can be considered as incompressible and can thus be described using the Navier–Stokes (NS) momentum equations and the continuity equation:

$$\rho(c) \frac{\partial \mathbf{U}}{\partial t} = -\nabla P + \eta \nabla \cdot \nabla \mathbf{U} + \rho_e \mathbf{E} - \rho(c)\mathbf{g}, \tag{5}$$

$$\nabla \cdot \mathbf{U} = 0, \tag{6}$$

where \mathbf{U} is the fluid velocity; $P = P(x, y, t)$ is the pressure, $\rho(c)$ and η are the density and the dynamic viscosity, respectively; $\rho_e \mathbf{E}$ is the electrostatic force applied to the fluid where

$\mathbf{E} = -\nabla \Phi$ is the applied electric field; and the final term $-\rho \mathbf{g}$ is the buoyancy produced from the variations in the density, where \mathbf{g} is the gravitational acceleration (Karaty et al. 2016). Using the Oberbeck–Boussinesq approximation, the fluid density ρ can be assumed to be a linear function of the salt concentration c as $\rho(c) = \rho_0 + \beta c$, where ρ_0 is the density of the fluid at the reference concentration c_0 , $c = (c_1 + c_2 + c_3)/3$ is the average ionic concentration, and β is the coefficient of the volumetric expansion.

Boundary conditions

Electrical double layers are overlapped on the nanochannel, which functions as having the same permselective effect as a membrane. The nanochannel only allows cations to pass through, indicating that the fluxes for the anions and particles are zero on the surface of the nanochannel network. Similar to a previous approach (Rubinstein and Zaltzman 2008), the concentration of cations at the surface of the nanochannel network is assumed to be at a fixed concentration in the nanochannel, and the electric potential at the network surface is assumed as a given low potential value V_{sur} due to the existence of the electrical double layers. In addition, it is assumed that the surface of the nanochannel network is impermeable to fluids and has a no-slip condition for the velocity and a zero-gradient condition for the pressure. Considering this, the corresponding equations describing the surface of the nanochannel network are given as follows:

$$\mathbf{J}_2 \cdot \mathbf{n} = \mathbf{J}_3 \cdot \mathbf{n} = 0; C_m = 2 \cdot C_0; \Phi = V_{\text{sur}}; \mathbf{U} = \mathbf{0} \tag{7}$$

where \mathbf{n} is the outward normal vector of the boundary surface.

As the channel walls are impermeable to ions, the fluxes for all particle species are considered to be zero. In addition, an electroosmotic slip boundary condition is utilized to simulate the EOF across the channel. For the EOF, it can be assumed that the channel walls meet the zero-gradient conditions for pressure. In summary, the corresponding boundary conditions for the channel walls can be expressed as

$$\mathbf{J}_i \cdot \mathbf{n} = 0; u_{\text{slip}} = -\epsilon \zeta(c) E_t / \eta \tag{8}$$

where the flow velocity at the channel walls u_{slip} is approximated by the Helmholtz–Smoluchowski electroosmotic slip equation, ϵ is the permittivity of the buffer solution, E_t is the tangential electric field, η is the viscosity of the solution, and the zeta-potential $\zeta(c)$ is related to concentration at the charged wall surface and can be expressed as $\zeta(c) = 20 \log_{10}(c_{\text{Na}^+})$ (Revil et al. 1999a, b).

The inlet of the microchannel is often connected to a reservoir; therefore, the ion concentrations and the pressure at the inlet can be assumed to be the same as those in the reservoir. A given electric potential V_L and zero-pressure

boundary conditions are utilized at the inlet of microchannel, giving the following corresponding equations:

$$C_1 = C_2 = C_0; \Phi = V_L; \nabla \mathbf{U} \cdot \mathbf{n} = \mathbf{0}; P = 0. \quad (9)$$

In addition, the boundary conditions for the microchannel outlet are assumed to be

$$\nabla C_i \cdot \mathbf{n} = 0; \Phi = V_R; \nabla \mathbf{U} \cdot \mathbf{n} = \mathbf{0}; P = 0. \quad (10)$$

Numerical methods and parameter setting

The presented theoretical model for the electrokinetic transport simulation can be expressed as Eqs. (1)–(6) together with the boundary conditions from Eqs. (7)–(10), which can be calculated using the finite element method. More details on this process can be found in Karatay et al. (2015). The computational domain is meshed using quadrilateral elements, where a finer grid size is applied near the surface of the nanochannel network as well as for the entrance and exit of the microchannel. The Poisson–Nernst–Planck (PNP) and NS equations are solved iteratively. At each time step, the PNP equations are solved using the velocity field from the previous step, and the volumetric electric force is then calculated and used to solve the NS equations. Since the voltage is slowly loaded in the experiment (Kim et al. 2009), a slowly increasing voltage is used to simulate this ICP phenomenon. The parameters used in the simulations are given in Table 1.

Before continuing into a detailed discussion, a simplified model is recalculated to validate the numerical process. By neglecting the surface voltage and no-slip boundary conditions caused by the nanochannel network, the presented theoretical model can be used to research a simplified model, as presented by Jia and Kim (2014). The comparison for the theoretical results from the presented model and that from the previous model is given in “Appendix A”. For this simplified model, an excellent agreement between the prediction from the proposed model and the previous model is

achieved. As a result, the presented numerical calculation process is considered to be valid.

Results and discussion

In this section, the multiphysics coupling mechanism for the micro–nanochannel concentration chip is numerically emphasized for a desalination plant and micromixer. The ion concentrations, flux and fluid velocities are all calculated. From the results, it is found that there is a strong fluid flow induced by the ICP near the surface of the nanochannel network. This ICP phenomenon can form an ion depletion zone or a mixing zone, where desalination or particle mixing is effectively attained. Therefore, this micro–nanochannel can be used for either desalination or a micromixing.

Model validation

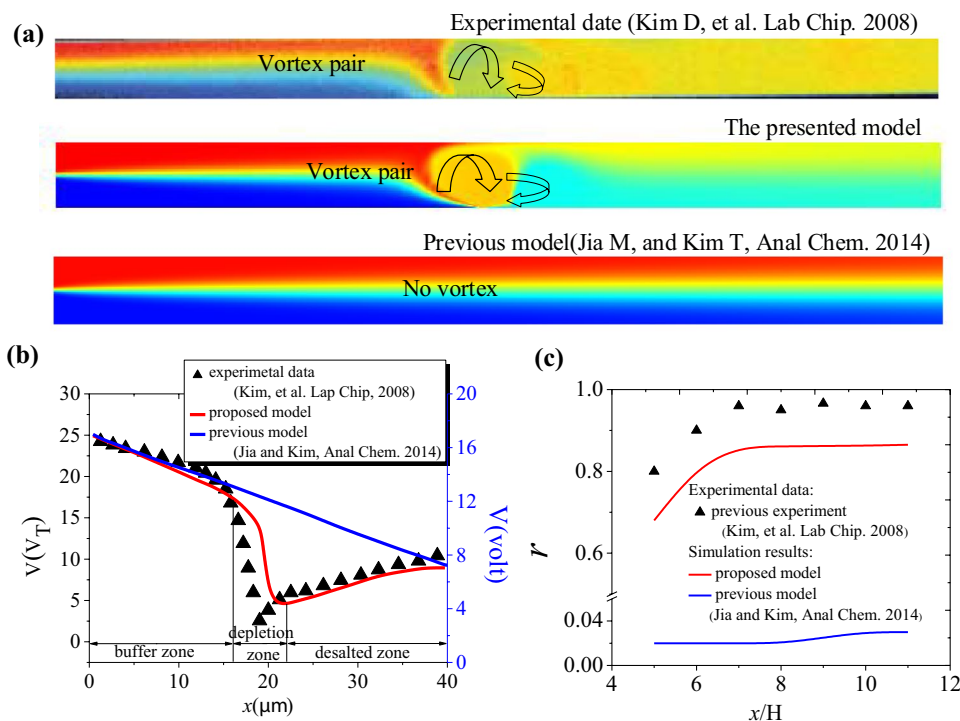
Direct measurements of the detailed flow and electric potential profiles (see Fig. 2b) within and near the depletion region were reported by Kim et al. (2009) Using micro-fabricated electrodes integrated with the microfluidic device, they measured the electric potential and electrical field at different points along the microchannel. The experimental results show that the electric potential dropped linearly in the buffer zone, had a drastic drop in the IDZ, and finally increased linearly in the desalted zone along the microchannel. We provide these same voltages as calculated using the proposed model and the previous model as a comparison, as shown in Fig. 2b. The previous theoretical results show that the electric potential decreases linearly along the microchannel, which is significantly different from the nonuniform distribution of the electric potential as measured from the experiments (Kim et al. 2009). However, the theoretical predictions from the presented model are considerably coincident with the experimental data. In comparison, it can be seen that our theoretical model can satisfactorily describe the nonuniform distribution of the electric potential for the micro–nanofluidic channel. With the formation of the IDZ and the space charge layer, the fluid accelerates and rotating vortices are generated at the micro–nanochannel interfaces. The non-equilibrium electrokinetic micro–nanofluidic mixer was proposed and its mixing performance was demonstrated by Kim et al. (2008). They directly measured the fluorescent intensity of particles along the microchannel, which reflect the vortex structure that leads to the mixing effect.

The theoretical predictions for particle mixing are generated using the proposed model and the previous model, as given in Fig. 2a. The theoretical predictions for micromixing using the previous model have evident differences with the experimental results (Kim et al. 2009). From the experimental results shown in Fig. 2a, c, there is a vortex pair structure

Table 1 Values for the parameter used in the simulations

Parameter	Value	Parameter	Value
L	110 μm	Z_1	+1
H	10 μm	Z_2	−1
L_m	5 μm	c_0	1 mM
T	300 K	V_{sur}	$4 \cdot V_T$
ϵ	$\epsilon_r(c)$	ζ	$\zeta(c)$
ρ	$\rho(c)$	V_T	26 mV
η	10^{-3} Pa s	ρ_0	1040 kg/m ³
D_1	1.34×10^{-9} m ² /s	ρ_s	1000 kg/m ³
D_2	2.03×10^{-9} m ² /s	β	70 kg/mol
D_3	1×10^{-10} m ² /s	c_m	2 mM

Fig. 2 **a** The experimental micromixing results in the micro–nanochannel (Kim et al. 2008) and the theoretical predictions from the presented model. **b** The electric potential distribution in the micro–nanochannel. **c** The normalized mixing index (r) along the channel, [red solid line: our theoretical prediction; blue line: theoretical results by Jia and Kim (2014); black solid line: experimental data (Kim et al. 2008)]



that enhances the mixing effect. However, in the theoretical results generated using the previous model, there is no vortex pair structure near the surface of the nanochannel network, indicating that it cannot produce the corresponding mixing effect when the length of the nanochannel network is around $4 \mu\text{m}$, as is used in real systems (Kim et al. 2009). In fact, when using the previous model (Jia and Kim 2014), a vortex structure, but not a vortex pair structure, can only be obtained when the length of the nanochannel network approaches $100 \mu\text{m}$, which is much larger than the actual length of the nanochannel network. In comparison, it can be seen that the theoretical predictions from the present model are considerably coincident with the experimental data when the length of nanochannel network is around $4 \mu\text{m}$ (Kim et al. 2009). Based on the comparisons with the experimental results for the voltage distribution (Kim et al. 2009) and the flow pattern (Kim et al. 2008), it is confirmed that introducing the surface voltage to describe the effect of the nanochannel network is necessary when performing simulations.

Time evolution of the IDZ under a tangential electric field

Figure 3a depicts the concentration distribution of ions in the micro–nanochannel at different stages. At the beginning ($t = 0 \text{ s}$), the ion depletion effect is not significant. This is because the energy barrier is relatively low, which leads to more ions that can pass through the area above the nanochannel network, leading to a lower desalination efficiency.

From Fig. 3a, it can be seen that the IDZ region begins to form after $t = 0.01 \text{ s}$. The ICP region gradually develops under the action of the EOF as time progresses, and the ion depletion zone forms in the downstream of the micro–nanochannel. As a result, effective seawater desalination can be achieved.

Figure 3b gives the ion concentration distribution at different times in the micro–nanochannel. It is seen that the anion concentration is nearly constant in the downstream of the micro–nanochannel. These theoretical results are in good agreement with the experimental and theoretical observations (Kim et al. 2009; Jia and Kim 2014). Figure 3c represents time evolution of the space charge density at the center line of the electrokinetic channel. For $t < 0.01 \text{ s}$, the space charge layer becomes thicker with t . However, for $t > 0.01 \text{ s}$, the space charge layer becomes thinner with time.

An interesting observation for the time evolution of the ion depletion length under tangential electric field conditions ($V_L > V_R$) is shown in Fig. 3d. It can be seen that the evolution of the depletion length varies nonlinearly (\sqrt{t}) with time for $t < 0.01 \text{ s}$. However, for $t > 0.01 \text{ s}$, a linear depletion thickness growth with a scaling of t is observed.

Generally, the extension velocity of the ion depletion layer can be defined as $U_s = dx_d/dt$. Here, x_d is the length of the ion depletion layer, as shown in Fig. 3a. In fact, the propagation velocity of the ion depletion layer within the microchannel is contributed to by the flux, as shown in Fig. 5c. Using this observation, the propagation velocity of the depletion layer can also be defined as $U_s = \mathbf{J}_i/c_i$. For

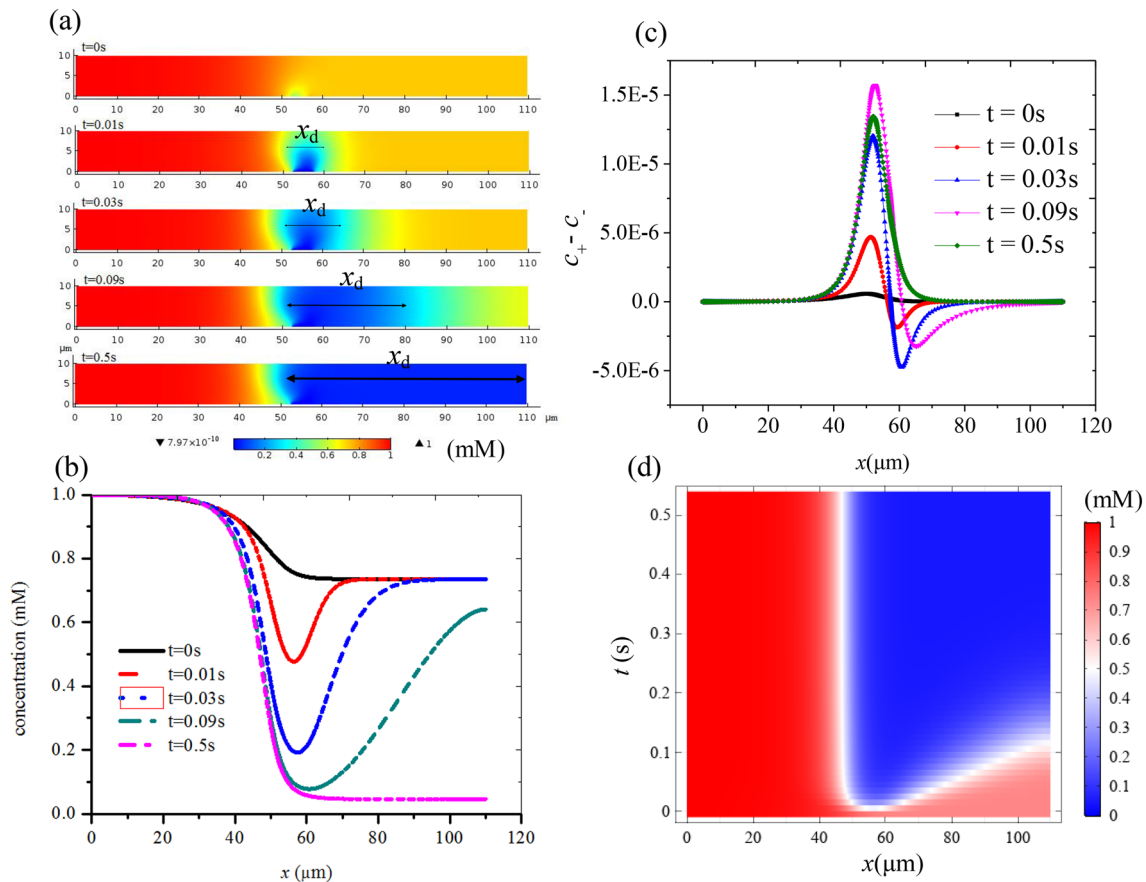


Fig. 3 Concentration of anions at different times. **a** 2D concentration distributions at $t=0, 0.01, 0.03, 0.09,$ and 0.5 s. **b** Profiles for the anion concentration along the center line of the micro-nanochannel. **c**

Space charge density along the channel at various times. **d** Time evolution for the propagation of the depletion zone

$t < 0.01$ s, the bulk flow has not yet developed, so it can be ignored. The flow of the fluid near the nanochannel network exhibits the second kind of EOF characteristics, which is consistent with previous reports (Li et al. 2017; Ouyang et al. 2018). Recently, the Demekhin group (Kalaïdin et al. 2010; Demekhin et al. 2011) reported that the flux of the IDZ near an ion selective surface has a self-similarity scaling law of $J(t) = 2j\sqrt{t}$, where j is the cation flux at the surface of the nanochannel network. Using this approximation, we derive a one-dimensional description for the IDZ propagation for $t < 0.01$ s as:

$$\frac{d}{dt}x_d = \mathbf{J}_i/c_i \sim j\sqrt{t}/c_i. \quad (11)$$

For $t < 0.01$ s, the EOF and vortex have not full developed, indicating that the convection flux can be neglected. Therefore, the diffusion flux of the nanochannel network surface can be satisfied by $j \sim O(j_0)$, where $j_0 = H/(2zeDc_0)$ is the diffusion flux. In addition, the ion concentration in the depletion layer is approximately proportional to the vortex height h_{EO_2} as $c_i/c_0 \sim h_{\text{EO}_2}/H$. This approximate relationship is

often used to estimate the concentration distribution of the depletion layer (Dydek et al. 2011). Therefore, the scaling law for the IDZ propagation can be simplified as $\frac{d}{dt}x_d \sim \sqrt{t}$. This observation is in a good agreement with our numerical results (see Fig. 3d).

It is worth noting that this scaling law is fundamentally different from the observations of Yu and Silber, which scales as t (Yu and Silber-Li 2011). To explain this discrepancy, Fig. 5c illustrates that the temporal and spatial variations in the flux approximately satisfy the self-similarity scale ($J(t) \sim 2j\sqrt{t}$) for $t < 0.01$ s at the diffusion regime. In the derivation of the Yu and Silber model, the time evolution of the flux is neglected and the total flux is considered to be a constant, which gives a linear growth that scales as t .

For $0.01 \text{ s} < t < 0.1$ s, the vortex is fully developed, and the depletion layer expands downstream of the channel to form a fully developed depleted zone. Therefore, we can think of the local electric field and the flow velocity as constant values. Using these approximations, one can obtain the following scaling law for the propagation velocity of the one-dimensional IDZ, where ζ is a constant:

$$\frac{d}{dt}x_d = \mathbf{J}_i/c_i = -\left(D_i \frac{\nabla c_i}{c_i} + Z_i \frac{D_i F}{RT} \nabla \Phi\right) + \mathbf{U} \sim J_{\text{const}} + u_{\text{slip}} \sim \zeta. \quad (12)$$

It can be seen from Eq. (12) that the scale for the propagation velocity of the depletion zone is a constant velocity ζ , which is in good agreement with our simulation results. In other words, in the one-dimensional description, the propagation velocity of the depletion zone is determined from the convection flux. However, it is interesting to note that the scaling law for the constant propagation velocity ζ is different from the scaling law given by Zangle et al. (2010) They found that the propagation of the IDZ also spreads as \sqrt{t} for a constant voltage model. To explain this discrepancy, it is necessary to analyze the experimental configurations and theoretical derivation process.

In the experimental configuration from Zangle et al., they designed micro-nanochannels with different heights, and the voltages were configured as $V_L = V_R$. The flux was conserved, flowed in from the channel inlet, passed through the nanochannel network, and finally flowed out of the microchannel exit. However, there was no tangential electric field ($V_L = V_R$) in their experiments or theoretical analysis. Then, the IDZ propagated to both ends (inlet and outlet) of the channel. In addition, their theoretical derivation neglected the effect of vortices near the nanochannel network to obtain the scaling law ($\sim \sqrt{t}$) for the IDZ propagation. However, when the voltage satisfies $V_L > V_R$, a tangential electric field forms at both ends of the channel, which affects the propagation of the IDZ due to the EOF. In addition, the vortex near the surface of the nanochannel network pushes and extends the ion depletion zone to downstream of the channel (see Fig. 3a). The flow speed at the outlet is proportional to the tangential electric field strength ($U \sim (V_L - V_R)/L$), and the vortex produces a linear pumping effect, which is consistent with our previous observations (Li et al. 2017). Therefore, the propagation velocity of the ion depletion zone is extended downstream of the channel due to the constant velocity under the tangential electric field.

Degree of desalination

Here, the factors for ICP desalination are investigated, including the effects of the buffer concentration, length and performance of the nanochannel network, height of the microchannel and tangential electric field on the desalination efficiency. The desalination effect is one of the most important applications of ICP systems. In this section, we consider the effects of different parameters on the desalination rate, which is instructive when optimizing the concentration chip. Figure 4a shows the effect of the left end voltage on the desalination rate given the same tangential electric field

($E = (V_L - V_R)/L$). It can clearly be seen from the figure that as the left end voltage V_L increases, the desalination rate of the system correspondingly increases. This is because the increased left end voltage allows more cations to pass from the micro-nanochannel interfaces, which then enhances the strength of the ICP. Figure 4b shows the effect of the concentration of the micro-nanochannels on the desalination rate, indicating that increase in the concentration causes the rate of desalination to decrease. This is because increases in the micro-nanochannel interface concentration result in a stronger concentration gradient near the micro-nanochannel interfaces, which enhances the local zeta potential and reduces the salt rejection.

The size parameters can significantly influence the ICP strength in the microchannel. Simulation results are given to show the effects of the nanochannel network length and the microchannel height for $V_L = 16V_T$, $V_R = 6V_T$, $V_{\text{sur}} = 4V_T$, and $c_0 = 1 \text{ mM}$. As shown in Fig. 4c, increasing the length of the nanochannel network corresponds to having more nanochannels. This enhances the cationic leakage, thereby growing the influential area of the ICP effect and increasing the desalination rate. When the number of nanochannels is fixed, it can be seen that the desalination rate decreases with an increase in the microchannel height. As the height of the microchannel increases, more ions can cross the potential barrier [see our previous publication (Li et al. 2017)], which results in a reduced salt rejection.

In addition, the buffer concentration has an important impact on the desalination rate. Figure 4c shows the relationship between the buffer and ion concentrations at the outlet. For the considered voltage configuration of $V_L = 16V_T$, $V_R = 6V_T$, $V_{\text{sur}} = 4V_T$, increasing the buffer concentration improves the desalination rate of the system. This is because a high concentration at the inlet can increase the electroosmotic slip velocity $\mathbf{U} = -\epsilon\zeta(c)E_t/\eta$ at the microchannel surface, which drives more ions from the water into the microchannel. The cations quickly leak to the nanochannel network, which leads to a depletion of the ions downstream of the microchannel. In addition, the illustrations in Fig. 4c compare the desalination effect under low and high buffer concentrations.

Mechanism of ICP desalination

Studying the ion dynamic in the micro-nanochannel is helpful to better understand the mechanism of ICP desalination. Figures 5c gives the flux distribution of the cations and anions, respectively, where the curves represent the streamline, the arrows represent the ion fluxes, and the arrow lengths are proportional to the size of the fluxes. From Fig. 8, it can be seen that the cations enter the micro-nanochannel at a high speed and leak from the nanochannel network, which results in only a small number of cations remaining in the water

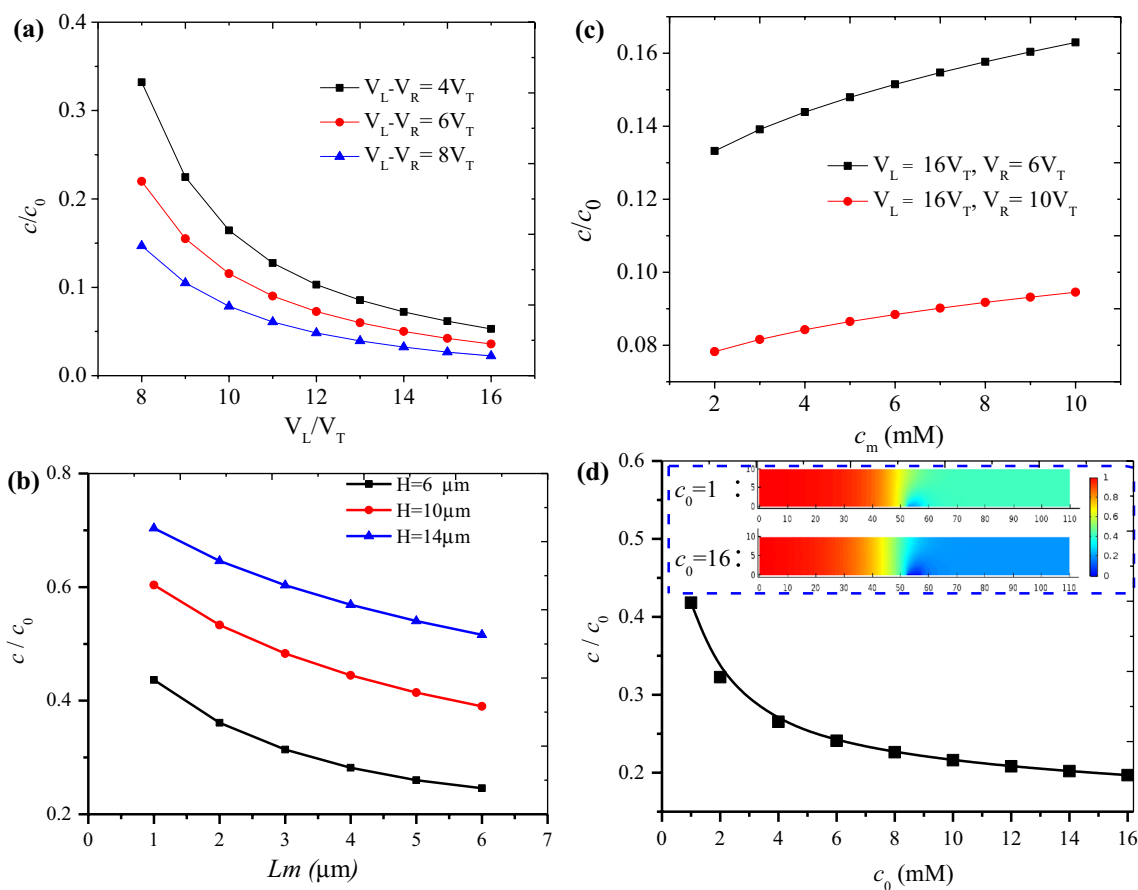


Fig. 4 Influential factors for the desalination process. **a** Effects of the tangential electric field. **b** Effects of a fixed microchannel with varying the nanochannel length. **c** Effects of the buffer concentration on

downstream of the micro–nanochannel. For the anions, the dynamic characteristics are relatively more complex. As shown in Fig. 3b, the cationic leakage is saturated at $t=0.5$ s. At this time, Fig. 3a shows that the anions are mainly trapped in the vortex of the micro–nanochannel and only a few can overcome the potential barrier and move downstream of the micro–nanochannel. In addition, the anions move into the micro–nanochannel with the fluid, but those in the vicinity of the micro–nanochannel wall are subjected to large forces from the electric field. This results in anions near the channel wall overcoming the water flow and entering the inlet of the micro–nanochannel.

Figure 5a, b shows the velocities of the water and ions over different cross-sections under a steady state when $t=0.5$ s. As can be seen from Fig. 5a, b, the cation velocity ($\mathbf{u}_i = \mathbf{J}_{i,x}/c_i$) is greater than that of the water, while the anion velocity is smaller. This is because the cations follow the fluid movement but are also driven by the electric field, which further increases their speed; however, the anion speed is weakened under the same electric field. By calculating the average velocity of the anions at the cross-section of

the desalination rate by comparing the desalination effect under two typical cases for different buffer concentrations. **d** Effects of the nanochannel network length and height of microchannel on salt rejection

the channel ($U_{Cl^-} = \int_{cs} U_1 dy/H \approx 0$), it is found that average speed of the anions is nearly zero at the inlet and outlet of the micro–nanochannel.

Figure 5c shows the average of the ion fluxes at the inlet and outlet of the electrokinetic channel at different times. It can be seen that in the steady-state conditions, the average flux of the cations at the inlet of the micro–nanochannel is 0.7×10^{-3} mol/(m²s) and at the outlet is 0.3×10^{-4} mol/(m²s). However, under the steady state, the average fluxes of the anions at the inlet and outlet of the micro–nanochannel are much smaller those for the cation fluxes, which are nearly zero. Referring further to the ion flux distributions in the microchannel given in our previous work (Li et al. 2017), it is found that cations enter the micro–nanochannel and pass through the surface of the nanochannel network, but there are almost no anions downstream of the micro–nanochannel. Therefore, this ICP micro–nanochannel can be used for desalination.

The effects of the nanochannel network performance on the desalination are studied. If nanotubes in the nanochannel network are sufficiently thin, they can induce

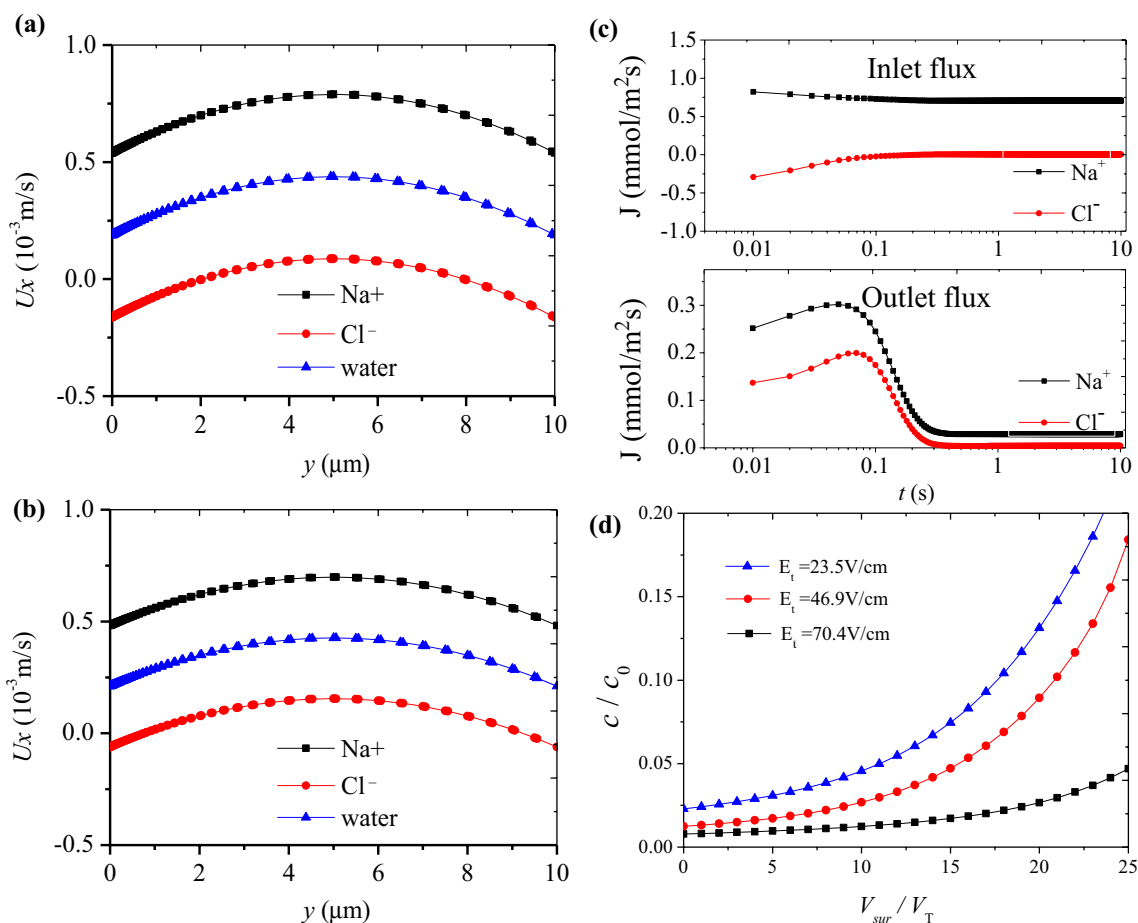


Fig. 5 Tangential velocity profiles of the cations, anions and water over different cross sections at **a** $x = 10 \mu$ m and **b** $x = 100 \mu$ m. **c** The average of the ion fluxes over the cross section at the inlet and out-

let boundaries. **d** The effect of the nanochannel network performance and tangential electric field on the desalination process

overlapping EDLs, which then produce an ideal ion-selective effect and a strong ICP. As there is an inverse correlation between the strength of the ICP effect and the voltage on the surface of the nanochannel network, it is necessary to introduce a surface voltage to describe the effect of the nanochannel network performance. This means that in the case of a low surface voltage, the performance of the nanochannel network improves, so the corresponding desalination rate increases, which is consistent with previous experimental results (Huang et al. 2016).

The effects of the tangential electric field on the desalination are also studied. When the characteristics of the nanochannel are constant, that is, when the surface voltage is fixed, the increasing tangential electric field improves the desalination performance. This is because the tangential electric field promotes cation leakage. In addition, when the nanochannel network performance improves, the effect of the tangential electric field on the desalination becomes relatively small. However, when the nanochannel

network performance is relatively poor, a larger tangential electric field is required to improve the desalination efficiency for the micro–nanochannel.

Electrokinetic mixing pump

As shown in Fig. 6a, there is a vortex pair near the surface of the nanochannel network, where its maximum velocity reaches ~ 4 mm/s. The anticlockwise vortex forms in the middle left of the nanochannel network because the fluid rapidly flows to the surface under the action of an electric field force. The vortex then moves upwards due to the existence of a local pressure near the nanochannel network. Finally, the vortex develops a rapid rotation. Similarly, there is also a reverse but weak electric field force near the middle right of the nanochannel network; thus, a clockwise vortex is formed with a lower intensity. The nonlinear vortex on the surface of the nanochannel network is a typical feature of this type of micro–nanochannel system. These theoretical

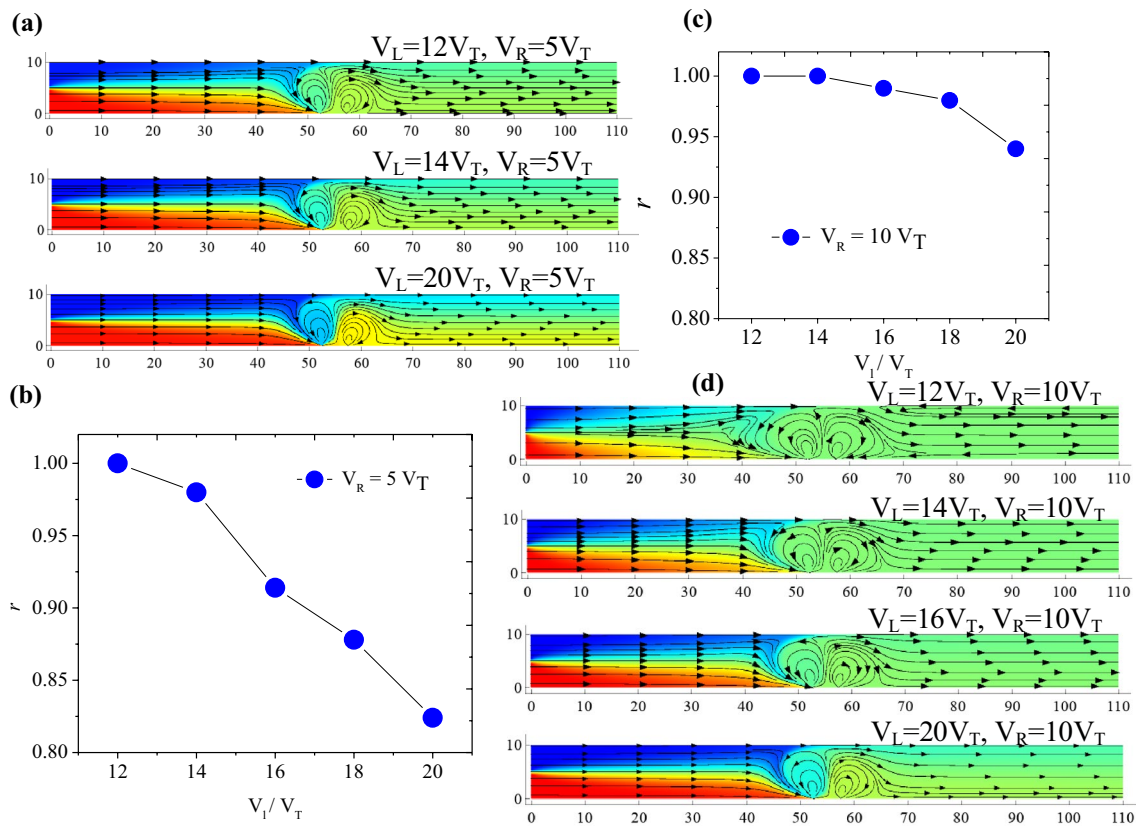


Fig. 6 Mixing results and the streamline distribution under different tangential electric field strengths. Parts **a** and **d** show the streamlines and particle concentrations. (The black lines and arrows show the

streamlines near the membrane in which a vortex is generated and the colors represent the distribution of the particle concentrations). Parts **b** and **c** show the mixing index under different left voltage conditions

results given in Fig. 6 are reasonably consistent with experimental and quantitative theoretical results (Kim et al. 2008).

This concise device can also effectively act as a micro-mixer pump. The definition of the mixed index (r) here uses that from a previous method (Kim et al. 2008). Figure 6a, d, respectively, shows the streamline distribution and mixing results of the microchannel under different tangential electric field strengths. Here, it is assumed that the concentrations of the two parallel liquid streams have different concentrations of 1 M/L and 10^{-4} M/L. As shown in Fig. 6b, c, the mixing effect of the particles decreases as the tangential electric field increases. This is because the tangential electric field enhances the vortex speed. However, the response time of the particle mixing is shortened, which results in a decreased mixing effect for the particles. Figure 6b, c shows the effects of the tangential electric field ($E_T = (V_L - V_R)/L$) on the mixing efficiency. It is seen that the mixing efficiency

reduces when the tangential electric field strength is too large. However, the mixing efficiency is close to the ideal value for low electric field intensities. Based on the above results, it can be found that an appropriate vortex intensity is needed for the particles to mix, and the optimal mixing efficiency reaches 99% as shown in Fig. 6b, c.

We also investigated the effects of the nanochannel width on the mixing efficiency. Figure 7a shows the effect of different tangential electric field strengths on the mixing efficiency. We find that as the strength of the tangential electric field increases, the mixing is further reduced. Figure 7b shows the relationship between the mixing efficiency and the left end voltage V_L and find that the mixing efficiency decreases linearly with the voltage.

To explain this linear pumping effect, we analyze the flow and pressure fields in the channel. Figure 7c, d, respectively, shows the pressure and average flow velocity

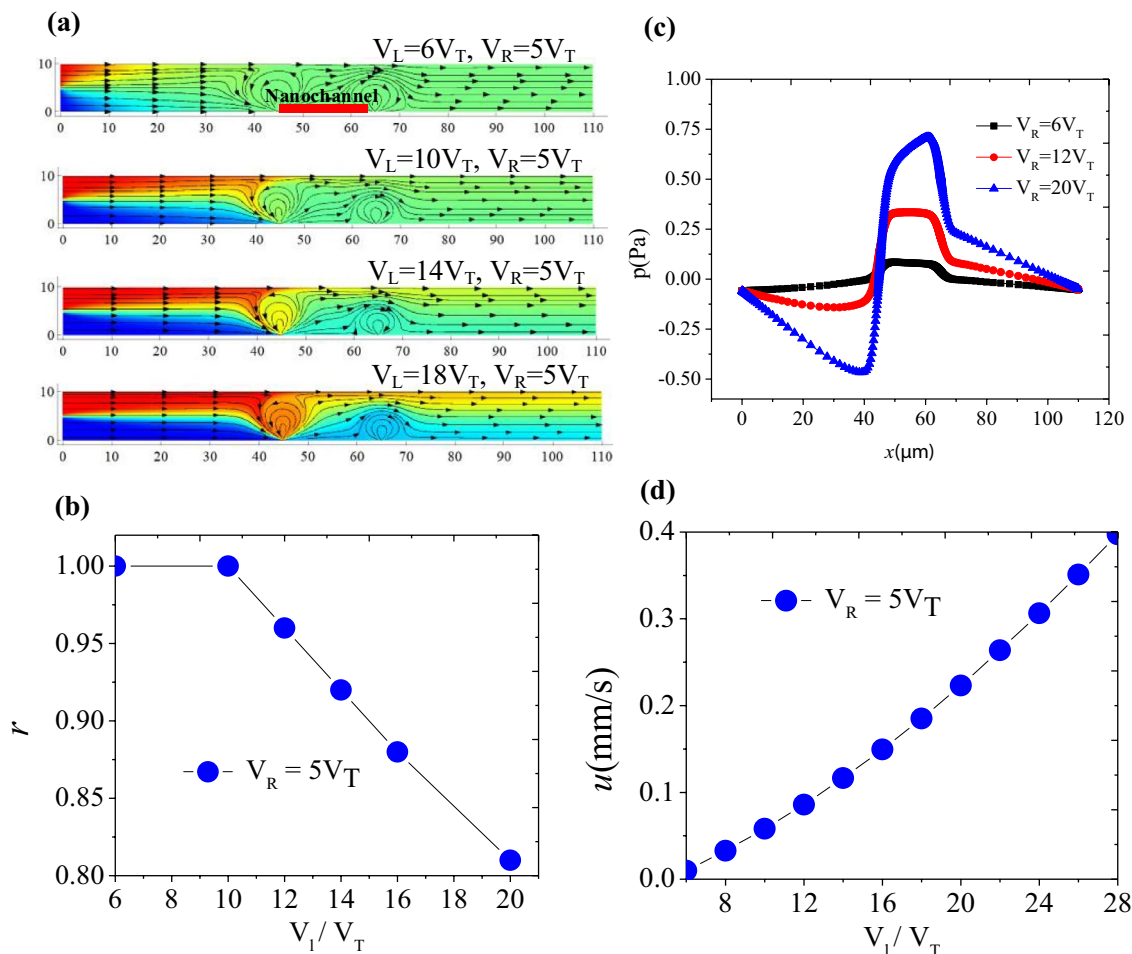


Fig. 7 Mixing results and the streamline distribution under different voltages. **a** Streamlines and particle concentrations. **b** Mixing index under different left voltage conditions. **c** Pump effect. **d** Average velocity

distribution within the channel. It is seen from the figure that the vortex near the nanochannel induces a linear pumping effect, which is consistent with our previous work (Li et al. 2017). This also means that the concentration-dependent zeta potential and the fixed concentration boundary can be used to describe the charged wall surface characteristics. Whence, the simplified boundary condition is considered to be reasonable. The average flow velocity and voltage have an approximately linear relationship, indicating the vortex intensity increases linearly. Consequently, this also leads to a linear decrease in the mixing efficiency.

Conclusions and outlook

Herein, a multiphysics coupling model is presented by introducing a fixed surface voltage to describe the effect of the nanochannel network and the concentration-dependent zeta potential to describe the amplified zeta potential near the micro–nanochannel interfaces. By neglecting the surface voltage boundary, the present theoretical model simplifies to the one presented by Jia and Kim (2014). For this simplified case, an excellent agreement between the predictions from the present model and the previous

model is achieved, which confirms the effectiveness of our computational process. In particular, comparing the results with experimental data for the voltage distribution (Kim et al. 2009) and the vortex streamlines (Kim et al. 2008) confirm that introducing the surface voltage to describe the effect of the nanochannel network is necessary. The main conclusions of the present study are as follows:

1. The scaling laws are linear (t) and nonlinear (\sqrt{t}) for the time evolution of the depletion zone propagation due to diffusion and convection fluxes, respectively.
2. The effects of the buffer concentration, length and performance of the nanochannel network, microchannel height and tangential electric field on the desalination degree are investigated. By changing these parameters, the salt rejection rate reaches up to 91%.
3. Detailed studies are performed to reveal the mechanism for ICP desalination. The average anion fluxes at the inlet and outlet of the microchannel are much smaller than the cation fluxes, which are nearly zero.
4. This concentration chip can also effectively act as a micromixer pump. By modifying the voltage configuration, the mixing efficiency reaches up to 99%.

This paper studies the mechanism for ion transport through micro–nanochannel interfaces. These results fully demonstrate the understanding of the ion transport and the time evolution for the propagating depletion zone at the micro–nanochannel interfaces. These conclusions provide an important guide to the design and optimization of concentration chips. The concentration chip can also be used for ions preconcentration (Wang et al. 2005; Sung et al. 2013) and deposition (Chen et al. 2016; Chen et al. 2017).

Acknowledgements This work was supported by the Natural Science Foundation of China (Grant Nos. 11972257, 11802225 and 11472193) and Natural Science Basic Research Plan in Shaanxi Province of China (Program No. 2019JQ-261). The authors gratefully acknowledge these supports. We also thank anonymous reviewers for their helpful comments on an earlier draft of this paper.

Appendix A: Numerical verification

See Fig. 8.

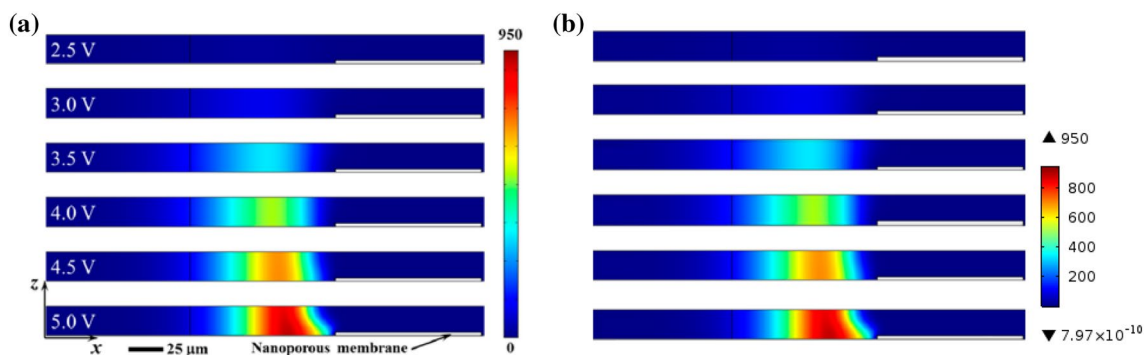


Fig. 8 Comparison of our presented results and the previous results. **a** Previous numerical results (Jia and Kim 2014). **b** Our presented numerical results

By neglecting the surface voltage boundary and no-slip boundary caused by the nanochannel network, the presented theoretical model can be directly compared to the simple model presented by Jia and Kim (2014) to prove the correctness of the numerical process. For this simplified case, an excellent agreement between the prediction from the present results and the previous simulation results is achieved. As a result, the present numerical calculation process has been validated.

References

- Chen Q, Jiang ZW, Yang ZH et al (2016) Differential-scheme based micromechanical framework for saturated concrete repaired by the electrochemical deposition method. *Mater Struct* 49(12):5183–5193
- Chen Q, Jiang ZW, Yang ZH et al (2017) Differential-scheme based micromechanical framework for unsaturated concrete repaired by the electrochemical deposition method. *Acta Mech* 228:415–431
- Chiu PH, Chang CC, Yang RJ (2013) Electrokinetic micromixing of charged and non-charged samples near nano–microchannel junction. *Microfluid Nanofluid* 14(5):839–844
- Choi E, Kwon K, Lee SJ et al (2015) Non-equilibrium electrokinetic micromixer with 3d nanochannel networks. *Lab Chip* 15(8):1794–1798
- Coelho D, Shapiro M, Thovert JF et al (1996) Electroosmotic phenomena in porous media. *J Colloid Interface Sci* 181(1):169–190
- Demekhin EA, Shelistov VS, Polyanskikh SV (2011) Linear and non-linear evolution and diffusion layer selection in electrokinetic instability. *Phys Rev E* 84(3):036318
- Demekhin EA, Nikitin NV, Shelistov VS (2013) Direct numerical simulation of electrokinetic instability and transition to chaotic motion. *Phys Fluids* 25(12):122001
- Deng DS, Wassim A, William AB, Bazant MZ et al (2015) Water purification by shock electro dialysis: deionization, filtration, separation, and disinfection. *Desalination* 357:77–83
- Druzgalski CL, Andersen MB, Mani A (2013) Direct numerical simulation of electroconvective instability and hydrodynamic chaos near an ion-selective surface. *Phys Fluids* 25(11):8316–8322
- Duan C, Majumdar A (2010) Anomalous ion transport in 2-nm hydrophilic nanochannels. *Nat Nanotechnol* 5:848–852
- Dukhin SS (1991) Electrokinetic phenomena of the second kind and their applications. *Adv Coll Interface Sci* 35(91):173–196
- Dydek EV, Zaltzman B, Rubinstein I et al (2011) Overlimiting current in a microchannel. *Phys Rev Lett* 107(11):118301
- Hlushkou D, Knust KN, Crooks RM, Tallarek U (2016) Numerical simulation of electrochemical desalination. *J Phys Condens Matter Inst Phys J* 28(19):194001
- Huang HN, Gao SB, Li X et al (2016) Microfluidic chips for effective desalination of seawater based on ionic concentration polarization. *Chin J Anal Chem* 44(12):1808–1813
- Jia M, Kim T (2014) Multiphysics simulation of ion concentration polarization induced by a surface-patterned nanoporous membrane in single channel devices. *Anal Chem* 86(20):10365
- Kalađin EN, Polyanskikh SV, Demekhin EA (2010) Self-similar solutions in ion-exchange membranes and their stability. *Dokl Phys* 55(10):502–506
- Karatay E, Druzgalski CL, Mani A (2015) Simulation of chaotic electrokinetic transport: performance of commercial software versus custom-built direct numerical simulation codes. *J Colloid Interface Sci* 446:67–76
- Karatay E, Andersen MB, Wessling M, Mani A (2016) Coupling between buoyancy forces and electroconvective instability near ion-selective surfaces. *Phys Rev Lett* 116(19):194501
- Kim SJ, Wang YC, Lee JH et al (2007) Concentration polarization and nonlinear electrokinetic flow near a nanofluidic channel. *Phys Rev Lett* 99(4):044501
- Kim D, Raj A, Zhu L et al (2008) Non-equilibrium electrokinetic micro/nano fluidic mixer. *Lab Chip* 8:625–628
- Kim SJ, Li LD, Han J (2009) Amplified electrokinetic response concentration polarization near nanofluidic channel. *Langmuir* 25(13):7759–7765
- Kim SJ, Ko SH, Kang KH, Han J (2010) Direct seawater desalination by ion concentration polarization. *Nat Nanotechnol* 5(4):297–301
- Lee J, Kim S, Kim C, Yoon J (2014) Hybrid capacitive deionization to enhance the desalination performance of capacitive techniques. *Energy Environ Sci* 7(11):3683–3689
- Li Z, Liu W, Gong L et al (2017) Accurate multi-physics numerical analysis of particle preconcentration based on ion concentration polarization. *Int J Appl Mech* 9(08):1750107. <https://doi.org/10.1142/S1758825117501071>
- Luo K, Wu J, Yi HL, Tan HP (2016) Lattice Boltzmann model for Coulomb-driven flows in dielectric liquids. *Phys Rev E* 93:1–11
- Luo K, Wu J, Yi HL, Tan HP (2018) Three-dimensional finite amplitude electroconvection in dielectric liquids. *Phys Fluids* 30:023602
- Mani A, Zangle TA, Santiago JG (2009) On the propagation of concentration polarization from microchannel–nanochannel interfaces. Part I: Analytical model and characteristic analysis. *Langmuir* 25(6):3898–3908
- Marino S, Shapiro M, Adler PM (2001) Coupled transports in heterogeneous media. *J Colloid Interface Sci* 243(2):391–419
- Mishchuk NA, Haldal T, Volden T et al (2009) Micropump based on electroosmosis of the second kind. *Electrophoresis* 30(20):3499–3506
- Nikonenko VV, Kovalenko AV, Urtenov MK et al (2014) Desalination at overlimiting currents: state-of-the-art and perspectives. *Desalination* 342(5):85–106
- Ouyang W, Ye X, Li Z et al (2018) Deciphering ion concentration polarization-based electrokinetic molecular concentration at the micro–nanofluidic interface: theoretical limits and scaling laws. *Nanoscale*. <https://doi.org/10.1039/C8NR02170H>
- Peng R, Li D (2015) Effects of ionic concentration gradient on electroosmotic flow mixing in a microchannel. *J Colloid Interface Sci* 440:126–132
- Pham VS, Li Z, Lim KM et al (2012) Direct numerical simulation of electroconvective instability and hysteretic current-voltage response of a permselective membrane. *Phys Rev E* 86(4 Pt 2):046310
- Revil A, Pezard PA, Glover PWJ (1999a) Streaming potential in porous media: 1. theory of the zeta potential. *J Geophys Res Atmos* 104(B9):20021–20031
- Revil A, Schwaeger H, Iii LMC et al (1999b) Streaming potential in porous media: 2. theory and application to geothermal systems. *J Geophys Res Solid Earth* 104(B9):20033–20048
- Rubinstein II, Zaltzman B (2000) Electro-osmotically induced convection at a permselective membrane. *Phys Rev E* 62(2 Pt A):2238
- Rubinstein I, Zaltzman B (2008) Electro-osmotic slip of the second kind and instability in concentration polarization at electro dialysis membranes. *Math Models Methods Appl Sci* 11(02):263–300
- Rubinstein I, Zaltzman B (2015) Equilibrium electroconvective instability. *Phys Rev Lett* 114(11):114502
- Shen M, Yang H, Sivagnanam V et al (2010) Microfluidic protein preconcentrator using a microchannel-integrated nafion strip: experiment and modeling. *Anal Chem* 82(24):9989

- Shi PP, Liu W (2018) Length-dependent instability of shear electroconvective flow: from electroconvective instability to Rayleigh-Bénard instability. *J Appl Phys* 124(20):204304
- Sung KB, Liao KP, Liu YL, Tian WC (2013) Development of a nanofluidic preconcentrator with precise sample positioning and multi-channel preconcentration. *Microfluid Nanofluid* 14(3–4):645–655
- Wang YC, Stevens AL, Han J (2005) Million-fold preconcentration of proteins and peptides by nanofluidic filter. *Anal Chem* 77(14):4293–4299
- Yeh LH, Zhang M, Qian S et al (2012) Ion concentration polarization in polyelectrolyte-modified nanopores. *J Phys Chem C* 116(15):8672–8677
- Yossifon G, Chang HC (2008) Selection of nonequilibrium overlimiting currents: universal depletion layer formation dynamics and vortex instability. *Phys Rev Lett* 101(25):254501
- Yu Q, Silber-Li Z (2011) Measurements of the ion-depletion zone evolution in a micro/nano-channel. *Microfluid Nanofluid* 11(5):623–631
- Zangle TA, Mani A, Santiago JG (2009) On the propagation of concentration polarization from microchannel–nanochannel interfaces. Part II: Numerical and experimental study. *Langmuir* 25(6):3909–3916
- Zangle TA, Mani A, Santiago JG (2010a) Effects of constant voltage on time evolution of propagating concentration polarization. *Anal Chem* 82(8):3114–3117
- Zangle TA, Mani A, Santiago JG (2010b) Theory and experiments of concentration polarization and ion focusing at microchannel and nanochannel interfaces. *Chem Soc Rev* 39(3):1014